R. & M. No. 3497

MINISTRY OF TECHNOLOGY

AERONAUTICAL RESEARCH COUNCIL

REPORTS AND MEMORANDA

The Subcritical Response and Flutter of a Swept-Wing Model

By C. A. K. Irwin and P. R. Guyett

LONDON: HER MAJESTY'S STATIONERY OFFICE

1968

PRICE 15*s.* 0*d.* NET

The Subcritical Response and Flutter of a Swept-Wing Model

By C. A. K. Irwin and P. R. Guyett

Reports and Memoranda No. 3497*
August, 1965

Summary.

The dampings and frequencies of the lower natural modes of oscillation of an aeroelastic, swept-wing model at wind speeds below its critical flutter speed have been deduced from measurements of the displacement-vector response of the model under sustained excitation. The flutter speed and frequency were also measured. The tests were done in a wind tunnel at low subsonic speeds. Calculations were made for comparison with the experimental results. Good agreement was obtained between the measured and calculated flutter speeds and frequencies, but the agreement on the response at subcritical speeds was less satisfactory. Turbulence in the wind tunnel led to difficulties in taking measurements, and comments are given on these and other problems that arise in determining response characteristics. The model was of a novel construction and its features are described.

LIST OF CONTENTS

*Replaces R.A.E. Tech. Report No. 65 186—A.R.C. 27 610.

1. *Introduction.*

For many years, wind-tunnel tests of aeroelastic models have been employed extensively to investigate the flutter characteristics of aircraft. These tunnel tests are made to define the flutter boundaries, and normally involve direct measurements of flutter speed and frequency; in recent years, however, attention[1] has been given increasingly to the possibilities of measuring the dampings and frequencies of the natural modes of oscillation of models below the critical conditions. The advantages of this type of test – usually termed measurement of subcritical response – are:

(1) It should be possible to predict the critical condition by extrapolation, thereby avoiding the risk of the model failing by flutter.

(2) The information obtained assists in a fuller understanding of the characteristics of the flutter, and enables a more extensive comparison to be made with predicted behaviour.

(3) The wind-tunnel results are of value in guiding and interpreting flight flutter tests made on aircraft.

(4) In wind tunnels where high levels of turbulence are present under certain operating conditions, the trends established by subcritical response measurements should show for any condition in which model failure occurs before response measurements are completed, whether the failure is due to an increase in turbulence or to a genuine aeroelastic instability.

Measurements of subcritical response in the wind tunnel can be done conveniently by applying a sustained sinusoidal excitation to the model and determining its resultant motion over ranges of frequency of oscillation. The main practical difficulties of measurement arise from unwanted excitation acting on the model. The consequent lack of accuracy in defining the response leads to uncertainties in analysing the results, and these uncertainties may be acute if the natural modes lie close together in frequency.

In view of the potential usefulness of subcritical response information, and of the possible difficulties of the type of experiment required, an investigation to gain knowledge of the problems involved has been made into the response characteristics of a model wing at low wind speeds. In addition to measurements of subcritical response, the flutter speed and frequency were measured directly. A comprehensive programme of calculations was carried through for comparison with the experimental results.

The model used in the tests was of a novel form of construction. For low-speed aeroelastic models of medium to high aspect ratio it is usual to employ a spar and box construction. With this method there are discontinuities in the profile of the model and a problem arises in providing, between the boxes, a seal having consistent damping and stiffness properties. In the new method, stiff chordwise members lying within the profile are attached to the spar and the resultant structure is covered with flexible plastic, foamed in position, which provides a continuous surface.

2. *The Applications of Vector-response Measurements.*

Methods of deducing the dynamic properties of a system from its vector response under steady sinusoidal forcing have been studied by Kennedy and Pancu[2], Broadbent and Hartley[3], Gladwell and Bishop[4], and Woodcock[5], amongst others. The usual technique is to determine the variation with frequency of the amplitude and phase of the motion of the system relative to the exciting force. In the neighbourhood of each of the natural frequencies of the system, the locus of the end of the displacement vector generally describes a curve that approximates to an arc of a circle. By assuming that the damping acting on the system is either hysteretic or viscous, it appears possible in principle, without knowing the absolute magnitude of the exciting force or the displacement, to obtain from this curve the frequencies of the natural modes, the decay rate in the modes, and – from a number of measurements of displacement – the shapes of the modes. The particular methods used to analyse the results of the experiments reported in this Report are described in Sections 4 and 5.

3. *Apparatus.*

3.1. *Wind Tunnel.*

The tests were made in the R.A.E. 5 ft open-jet wind tunnel.

3.2. *Model.*

The model was a half-span, straight-tapered wing of root chord 21 in., tip chord 6 in. and semi-span 36 in. with a leading-edge sweepback of 28 deg 47 min; the wing section was RAE 101 of thickness/chord ratio 0·10.

The model was built with a light alloy spar to which 18 light alloy segments were attached. Fig. 1a shows the assembly, and Fig. 2 and Table 1 give the dimensions of the segments and spar. The spar and segments were covered by solid Flexalkyd plastic foam. The plastic was foamed in position with the metal components supported in a mould of the external shape of the wing. Fig. 1b shows the complete model.

The plastic foam made a significant contribution to the stiffness of the model and this contribution is important because it has been shown[6] that the stiffness of the plastic depends upon the absolute humidity of the surrounding air; tests have also indicated that the dynamic stiffness of the plastic is greater than its static stiffness. Similar effects have been observed in measurements on Xylonite[7]. After casting, the stiffness of the plastic foam was reduced by working; this process, which was done manually, appears to remove local regions of high stiffness in the structure of the foam. The working was continued until measurements showed that the model stiffness had been brought down to a stable level, although this level varied with absolute humidity. Subsequent measurements of the displacement and twist of the wing in the line of flight under steady loading applied at a section 0·694 of the semi-span from the root indicated that the ratio of the flexural stiffness of the complete model to that of the metal structure before foaming was 1·10, and that the corresponding ratio of torsional stiffness was 1·60. Over a period of a year the natural frequency of the fundamental torsion mode of the wing varied within the range 14·1 c/sec to 15·0 c/sec, and it was found that the normal day-to-day variation in the frequencies of the modes in still air was of the order of 1·5 per cent.

3.3. *Model Support.*

The model was mounted vertically, tip upwards, by bolting and clamping a plate extending from the root of the spar (*see* Fig. 1a) to a substantial metal structure. A reflector plate, with a cut-out for the root support members, fitted against the base of the wing. In planform the reflector plate was 30 in. wide normal to the plane of the wing and 60 in. long, including a semi-circular nose. The level of the surface of the plate was 3 in. above the lowest point of the nozzle of the wind tunnel. The arrangement is shown in Fig. 4.

3.4. *Excitation.*

A small electrodynamic exciter with a permanent magnet field was connected to the wing aft of the spar at the section 7 in. from the root by a light rod having flexible wire couplings at each end. This exciter remained attached to the wing throughout the tests and thus effectively increased the inertia and structural stiffness of the model. Driving current in the coil of the exciter was obtained by amplifying the signal from a decade oscillator; the current was measured by determining the voltage developed across a resistor connected in series with the exciter coil.

3.5. *Instrumentation.*

Strain gauges were attached to the spar of the model at stations close to the root and at 0·6 of the semi-span from the root. Leads were provided enabling each set of gauges to be connected externally into a Wheatstone bridge sensitive to the local bending or twist of the spar.

In certain tests a miniature accelerometer was fixed to the model by cutting away a portion of the plastic foam and making a connection to the metal structure; the positions used were 19 in. from the root and 10·5 in. from the leading edge, and 25 in. from the root and 8·5 in. from the leading edge. The accelerometer was of a type developed by Instrumentation Department, R.A.E. especially for aeroelastic model tests; its size was 0·59 in. × 0·25 in. × 0·125 in. and it weighed 0·005 lb, which was small in relation to the weight of the segments of the model.

Some measurements of the displacement of the model in still air were taken using a vibration meter which detected changes in capacitance between discs of copper foil glued to the surface of the model and a probe held close to the face of the discs.

The method of treating the output signals from the strain gauges, accelerometer and displacement probe is shown diagrammatically in Fig. 5. Each of these signals was converted to a form acceptable to the measuring instrument; its amplitude and phase were then found relative to a reference signal proportional to the current in the coil of the electrodynamic exciter.

For the comparative measurements of signal amplitude the accuracy of the instruments was ± 2 per cent overall at full scale deflection; the corresponding accuracy of phase measurement was ± 1 deg. The accuracy achieved in the tests was dependent upon the steadiness of the signal levels: in the measurements of response in still air the signal levels were sufficiently steady to take full advantage of the instrument accuracy, but in certain conditions with the wind on the signal levels fluctuated considerably and consequently the accuracy was reduced (*see* section 8.1.).

4. *Measurements and Analysis of Response in Still Air.*

4.1. *Test Procedure.*

The model was prepared with a set of discs of copper foil fixed to its surface. Two discs were attached to each of the eighteen sections of the wing, at stations 0·25 and 0·80 of the local chord aft of the leading edge, as shown in Fig. 3. The displacement probe, which was required to be held close to the face of these discs, was mounted in a framework which enabled it to be placed accurately beside the discs. With the probe held in position at a measuring station, the test procedure was as follows:

(i) At each frequency the amplitude of the current in the coil of the exciter was adjusted to a convenient level; this level was maintained throughout the investigation of each mode giving an effectively constant amplitude of the input force.

(ii) A measurement was made of the amplitude of the signal from the vibration meter.

(iii) A measurement was made of the phase angle between the output signal from the vibration meter and the reference signal derived from the current in the coil of the exciter.

Readings were taken at a sufficient number of stations and frequencies to determine the displacement response in the first six modes. The way in which these results were analysed is described in the following Sections.

4.2. *Determination of Resonant Frequencies and Mode Shapes.*

For each mode and for each measurement station on the wing curves were drawn showing the variation with frequency of the magnitude and phase angle of the displacement vector relative to the exciting force. Circles were then fitted to these curves. The construction is illustrated in Fig. 6.

From the set of circles obtained in each mode the circle was selected which approximated most nearly to the vector response of a single degree of freedom system with hysteretic damping; for such a system the locus of the end of the response vector is a circle, the centre having zero displacement in phase with the exciting force and the circumference passing through the origin. Next, a position was chosen on this circle at which the indicated change of frequency with arc length was a minimum. The frequency at this point was taken as the resonant frequency of the mode*. It should be noted that the resonant frequency defined in this way could not be determined with great precision.

In the highest two measured modes (modes 5 and 6), and to a lesser extent in the fundamental torsion mode (mode 3), the positions of the constructed circles at nearly all of the measuring stations did not correspond at all closely to the position of the circle in the single-degree-of-freedom case. It follows that the forcing applied to the wing (at a single, fixed position) was not able to excite separately the pure normal modes of system.

---

*With hysteretic damping the resonant frequency occurs strictly at the point at which $\omega d\omega/ds$ is a minimum, where ω is the circular frequency and s is the distance along the vector curve; with viscous damping the resonant frequency occurs approximately at the point at which $1/\omega \,.\, d\omega/ds$ is a minimum. When the damping is low the minimum of $d\omega/ds$ occurs at practically the same point as the minimum of $\omega d\omega/ds$ and $1/\omega \,.\, d\omega/ds$.

In circumstances such as these it is necessary to enquire whether the chosen resonant frequencies are the frequencies of the normal modes, and whether it is possible from the measured vector responses to deduce the shapes of the normal modes. A set of mode shapes can be obtained by assuming that the normal mode displacement at each measuring station is proportional to the diameter of the constructed circle*. This supposes that the difference between the response in the required normal mode and the actual response is due to the forced response in the other modes of the system, and that the effect of this forced response upon the magnitude and phase of the response at each station remains constant over the range of frequency corresponding to the parts of the vector response curves through which the circles are constructed. Mode shapes found in this way are shown in Figs. 7 to 9. One method of checking these results is to examine the orthogonality of the modes.

The calculation of the inertia coefficients to check the orthogonality of the modes requires a knowledge of the distribution of the inertia of the model. This information was found partly by measurement and partly by estimation (*see* section 7.1.2.); the errors involved in this progress are difficult to assess precisely but are thought to be small. Taking the inertia data (Table 2) in conjunction with the modal data (Figs. 7 to 9) yields the matrix of generalised coefficients given in Table 3. Table 4 gives the corresponding coefficients $a_{rs} / \sqrt{a_{rr}\, a_{ss}}$ where a_{rs} is the cross-inertia coefficient for modes r and s, and a_{rr} and a_{ss} are the direct inertia coefficients for modes r and s respectively. With the exception of the cross inertia between modes 5 and 6, the value of the maximum cross-inertia coefficient is $7\frac{1}{2}$ per cent. The high value of the cross-inertia coefficient for modes 5 and 6 (19·9 per cent) suggests that, owing to the close proximity of the frequencies for these modes, the method of analysis was not able to separate the required orthogonal modes; thus each of the identified modes was a combination of the two orthogonal modes.

Making the assumption that the errors in the estimated distribution of inertia are small, the generally low values of the cross-inertia coefficients indicate that the deduced mode shapes are reasonably accurate.

Turning to the question of whether the chosen resonant frequencies are the frequencies of the normal modes, it is probably fair to argue that if the mode shapes are reasonably accurate then the frequencies associated with them are reasonably accurate also.**

4.3. *Determination of Direct Damping in the Modes.*

The direct damping in each of the first six modes was found by assuming that the parts of the vector response curves through which circles were constructed may be treated as the response of a system with a single degree of freedom.

It is usual to write the equation of motion of a system with a single degree of freedom under sustained sinusoidal forcing in one of the two following general forms:

$$a\,\ddot{q} + e(1 + ig)q = F\,e^{i\omega t}, \tag{1}$$

$$a\,\ddot{q} + d\dot{q} + eq = F\,e^{i\omega t}, \tag{2}$$

*In relation to their usefulness for deducing normal modes from vector response plots, an assessment is made in Ref. 8 of the method described in the present Report and of two alternative methods (these are based on the length of the quadrature vector and on the total vector length at the chosen resonant frequency); of these three methods it is shown that for the particular results under discussion in the present Report the method of analysis based on the diameters of the constructed circles gives the best approximation to the required orthogonal modes.

**From Rayleigh's method it follows that the errors in frequency should be smaller than the errors in mode shape, but it is not easy to establish the relative effects of these two types of errors upon predictions of the behaviour of the model.

where a is an inertia coefficient,

e is a stiffness coefficient,

d and g are damping coefficients,

q is a generalised co-ordinate,

F is a generalised exciting force,

ω is the angular frequency of oscillation.

In the first of these two forms the damping is hysteretic, i.e. it varies in phase with the velocity but with an amplitude that is proportional to the amplitude of the displacement. In the second form the damping is viscous, i.e. directly proportional to the velocity.

Referring to Fig. 6, if ω_R is the undamped natural frequency of the system, and ω_A and ω_B are two adjacent frequencies, such that $\omega_B < \omega_R < \omega_A$, and the arcs ω_A to ω_R and ω_R to ω_B subtend equal angles θ at the centre of curvature, then it may be shown that with hysteretic damping,

$$\frac{(\omega_A-\omega_R)}{\omega_R}\left\{2+\frac{(\omega_A-\omega_R)}{\omega_R}\right\}\cot\frac{\theta}{2}=\frac{(\omega_R-\omega_B)}{\omega_R}\left\{2-\frac{(\omega_R-\omega_B)}{\omega_R}\right\}\cot\frac{\theta}{2}=g. \tag{3}$$

$$\text{Provided } \frac{\omega_A-\omega_B}{\omega_R} \text{ is small, } \omega_R-\omega_B=\omega_A-\omega_R.$$

A value for the hysteretic damping coefficient, g, can therefore, be found from the vector response curves, and by examining the variation of the value of g with θ, on each side of ω_R, some indication can be obtained of how accurate a representation the theoretical model specified in equation (1) is of the actual system.

When the damping in a system is small it is possible to find a value for the viscous damping coefficient, d, which would give a vector response curve practically indistinguishable from the response curve with hysteretic damping; the relationship is:

$$g=\frac{d}{\sqrt{ae}}. \tag{4}$$

In this circumstance, the coefficient g can also be expressed in terms of the quantity C/C_c, the ratio of the actual velocity damping in the system to the critical damping required to change the free motion of the system from periodic to aperiodic, as follows:

$$\frac{C}{C_c}=\left(\frac{d}{2\sqrt{ae}}\right)=\frac{g}{2}. \tag{5}$$

Values of the ratio C/C_c deduced from vector response curves for each of the first six modes are given in Table 5.

5. *Measurements and Analysis of Subcritical Response.*

5.1. *Test Procedure.*

Measurements were made of the response of the model to sustained excitation at windspeeds in the range from 40 to 165 ft/sec. The procedure was to hold the windspeed constant, and then follow the steps (i) to (iii) described in Section 4.1., taking readings of the signals from the strain gauges or from the

accelerometer instead of from the vibration meter. At speeds up to 120 ft/sec. the response in the five lowest modes was investigated, but beyond this speed difficulties met in the experiment made it desirable to concentrate on the three lowest modes, since these had the most interesting characteristics, and appeared to be the most rewarding for study in the time available.

The experimental difficulties were due primarily to lack of smoothness in the windstream, which, at speeds above about 120 ft/sec., contained a powerful source of excitation in the model frequency range arising from vortex shedding at the nozzle of the open-jet wind tunnel. The presence of this unwanted periodic forcing produced a serious distortion of the vector response curves, in particular those for the third mode, rendering them incapable of meaningful interpretation. In an attempt to reduce the disturbance, a set of twelve 'fingers', each $1\frac{1}{2}$ inches in width normal to the flow and projecting $1\frac{1}{2}$ inches into the stream, were spaced evenly around the tunnel nozzle. This measure appeared largely to eliminate the periodic content of the flow disturbances, but had the effect of raising the level of the random turbulence. Fig. 10 presents results from a subsidiary experiment aimed at showing the spectrum of variation in the flow direction; this experiment was fairly crude but confirms the observed behaviour of the model.

Although it was necessary to reduce the periodic disturbances, the subsequent high level of random turbulence in the windstream led to grave problems in measuring the displacement vector response. The instrument which was used for this required a number of adjustments, some of which were extremely difficult to achieve with precision, since the transducer outputs fluctuated so widely and the fluctuation showed up on the instrument. Readings were taken at as high a level of forcing as practicable with the equipment used, to achieve the greatest ratio of signal to noise.

As a consequence of the difficulties of measurement, the determination of response became extremely tedious over the range of speeds above about 120 ft/sec. Although consistent vector response curves were obtained for each mode throughout the speed range, the time taken over these measurements had the effect of limiting the number of transducer signals that could be examined. Readings were taken of what appeared to be the most favourable strain gauge outputs, and of the accelerometer output at two positions on the wing (*see* Fig. 3).

At speeds close to the critical flutter speed, the low damping in two of the modes together with the high level of turbulence gave rise to a further problem. The electromagnetic exciter had a working amplitude of travel of $\pm\frac{1}{8}$ inch, and, in order to safeguard the coil suspension, stops were fitted to prevent greater movement. As the critical speed was approached turbulence caused the exciter to strike the stops intermittently, thereby upsetting the measurement of the model response. This behaviour made it impossible to determine the vector response above a speed of 162 ft/sec.

5.2. *Determination of Modal Frequencies and Dampings.*

The analysis of the vector response curves to yield modal frequencies and dampings followed the general lines of the procedure outlined in Sections 4.2. and 4.3. Circles were fitted to the curves in the neighbourhood of the resonant frequencies, and attempts were then made to identify these frequencies by finding the points on the curves corresponding to the minima of the quantity $d\omega/ds$, or, in cases where the damping was high, $1/\omega \,.\, d\omega/ds$*. Owing to scatter in the results it proved impossible to determine the frequencies with great accuracy, the accuracy varying both with the quality of the response curve and the damping in the mode.

For a linear system with viscous damping, it can be shown[5] that the resonant frequencies in the foregoing way are related to the roots of the equation describing the free response of the system. If the free response is written $q = \bar{q}\, e^{(\mu + i\nu)t}$, then

$$\omega_{Rr}^2 = \mu_r^2 + \nu_r^2 \tag{6}$$

*The form, $1/\omega \,.\, d\omega/ds$, appropriate to viscous damping, was preferred to the hysteretic damping form, $\omega d\omega/ds$, because the dissipative forces in the system were largely aerodynamic in origin.

where μ_r, ν_r are the roots of the rth mode of free motion,

q is a generalised co-ordinate,

t is time, and

ω_{Rr} is the chosen resonant frequency for mode r.

The quantity μ_r, which is a measure of the growth of the free motion of the system, may be found by means of a relationship, given in Ref. 5, which requires the values of some quantities which can be found readily from the response curve by geometrical construction. μ_r can be expressed in terms of the fraction of critical damping, C/C_c, as follows:

$$\frac{\mu_r}{\omega_{Rr}} = \frac{C}{C_c}. \tag{7}$$

Having found ω_{Rr} and μ_r, the value of ν_r is given by equation (6). ν_r is the angular frequency of the free motion of the system; the frequency in cycles per second, $\nu_r/2\pi$, is written n_r.

Since the objective of the response tests is to find the characteristics of the free motion of the system, the results of the analyses of the response curves are presented in the form of the values n_r and C/C_c. The variation of n_r and C/C_c with windspeed for the first 6 modes of the model is shown in Figs. 11 to 16.

In some instances, the figures give a band of value for the damping and frequency. This is because the response curves did not permit of a unique interpretation. Generally, for a chosen resonant frequency, the damping was found for each frequency point on the part of the curve which followed the constructed circle; this was sometimes on one and sometimes on both sides of the resonant frequency. Variations in the value of the damping can be taken as an indication of one or more of the following:

(i) Turbulence made it impossible to determine the true response curve.

(ii) The particular transducer did not give a clear picture of the response in the mode.

(iii) The exciter was poorly placed to force the mode.

With regard to (iii), it should be noted that since the mode changes with windspeed, a position for the exciter that is satisfactory in still air is not necessarily satisfactory throughout the speed range; the only certain ways of overcoming this difficulty are either to provide an arrangement for altering the position of the exciter without affecting the dynamic characteristics of the system, or alternatively, to provide several exciters; the first of these alternatives is difficult to achieve and the second adds considerably to the complexity of an experiment.

6. *Flutter Tests.*

The critical flutter condition was found by increasing the windspeed in small steps and at each speed observing the rate of decay of the motion of the model following a disturbance applied manually by jerking a cord attached to the model. Care was taken to keep the disturbance to a minimum in an attempt to prevent the exciter hitting the stops. In the presence of a large amount of turbulence, and with a small permissible travel of the exciter, it was not easy to determine the flutter speed accurately. At various times during the experiment critical speeds were measured in the range from $163\frac{1}{2}$ ft/sec to 173 ft/sec, but this variation was probably due mainly to the variation with absolute humidity of the stiffness of the plastic foam covering on the model; this phenomenon is discussed in Section 7.4.

The frequency of the flutter oscillation was determined by connecting the output from the strain gauges on the model to the Y plates of an oscilloscope, and then adjusting the frequency of an oscillator connected to the X plates until a steady Lissajous figure was obtained.

7. *Calculations of the Subcritical Response and the Flutter Condition.*

The equations of motion of the system were derived by applying Lagrange's equation[9]. The degrees of freedom chosen and the preparation of the coefficients are described in Section 7.1. Two sets of calculations were made: in one the subcritical response measurements were simulated using an analogue computer and in the other the roots of the equations of free motion were found using a digital computer; these approaches are described in Sections 7.2. and 7.3. respectively. Section 7.4. gives a description of some calculations of the effect upon the flutter condition of changes in stiffness of the model due to changes in the absolute humidity of the air.

7.1. *Preparation of the Coefficients.*

7.1.1. *Mode shapes.* The shapes of the first six modes of the model deduced from the measurements of response in still air were taken as the degrees of freedom of the system. These modes are shown in Figs. 7 to 9. It was assumed that the segments of the wing (*see* Section 3.2.), which were very stiff, remained rigid in the chordwise direction in all the tests.

7.1.2. *Model inertia.* Before final assembly to the spar, measurements were made on each of the metal segments to determine its mass, mass moment and moment of inertia about an axis in the plane of the wing normal to the line of flight. The moments of inertia were found from the results of tests in which the segments were mounted in turn on a spring-restrained vertical axle and a record was taken of the resultant frequency of oscillation; the effective stiffness and inertia of the axle were determined from the variation of frequency produced by adding masses of known inertia. The wing was then divided into sections 2 inches in span, each section containing one segment, and the contribution of the plastic foam and the spar to the inertia of the sections was calculated from measurements of the average density of the foam and metal and the geometry of the wing, making the assumption that the density of the foam was uniform. The total mass, position of the centroid and the radius of gyration in pitch about the centroid of each section are listed in Table 2.

The generalised inertias in the chosen degrees of freedom were subsequently found from the mass data and the mode shapes, and are shown in Table 3.

7.1.3. *Model stiffness.* The direct stiffness term in each degree of freedom was calculated from the generalised inertia and the mode frequency; the frequencies are given in Table 5. The cross-stiffness terms were set to zero in all calculations. This step was justified by some calculations made on the analogue computer, in which the critical conditions were found both with and without the cross-inertia coefficients; the results showed that the critical conditions were not affected significantly by the presence of the cross-inertia terms, and from this it was reasoned that the calculated response would also not be affected by the inclusion of the unknown cross-stiffness terms.

7.1.4. *Model structural damping.* The values of the direct dampings for each mode found from the results of the still-air response measurements (*see* Section 4.3.) were used. These results were converted into the equivalent viscous damping form to suit the analogue and digital calculation procedures. Table 5 lists the coefficients. All structural cross-damping coefficients were assumed to be zero.

7.1.5. *Oscillatory aerodynamic forces.* The oscillatory aerodynamic-force coefficients were found by means of the Mercury Digital Computer Programme RAE 161A prepared by D. E. Davies. This programme gives the generalised aerodynamic coefficients for a wing oscillating harmonically in rigid or flexible modes at subsonic speeds. In making the calculation, four displacement and upwash points were taken along the chordline at each of ten spanwise stations on the half wing. Values of the coefficients were determined for a number of frequency parameters.

7.2. *Determination of Subcritical Response using an Analogue Computer.*

Curves of the vector response of the model represented as a system with six degrees of freedom were obtained using the RAE Flutter Simulator[10]. The equations of motion were set up on the simulator and forcing was applied from an external oscillator; the amount of forcing in each degree of freedom was arranged to be in proportion to the generalised force produced by an exciter acting on the wing in the

position used in the wind-tunnel tests. Signals proportional to the displacement of the wing at the accelerometer positions or proportional (approximately) to the strain in the spar at the strain-gauge positions were obtained by adding vectorially a proportion of the displacement in each degree of freedom. The complete system thus represented an analogue of the wing, exciter and the acceleration and strain-gauge transducers. Measurements were taken of the phase and amplitude of the outputs from the simulated transducers over a range of frequency of forced oscillation at simulated wind speeds up to the critical flutter condition. In these tests the aerodynamic coefficients were kept constant and corresponded to a frequency parameter* of 0·26. Frequencies and dampings for the first three modes are plotted against windspeed in Figs. 18 to 21.

7.3. *Calculations of the Free Motion of the Wing.*

A digital computer was used to calculate the roots of the equations of free motion of the wing. These roots give the rate of growth or decay and the frequency of the natural modes of oscillation. The procedure was to insert into the equations the aerodynamic coefficients for a particular value of frequency parameter and then find the roots over a range of windspeed. Further calculations were made using the aerodynamic coefficients for other fixed values of frequency parameter. This was continued until for each mode it was possible to construct curves of the variation of rate of decay and frequency with windspeed that passed through several points at which the frequency parameters based on the calculated frequency of oscillation and the windspeed were equal to the frequency parameters assumed in the calculations. Fig. 22 illustrates the variation with windspeed of the rate of decay (expressed in the form of the fraction of critical damping – *see* equation (7)) in the 3rd mode (beginning as fundamental torsion in still air) for several values of the frequency parameter; circles on the curves indicate the points at which the assumed and calculated frequency parameters agree. (It should be noted that the variation of the rate of decay of the motion with the assumed frequency parameter was much larger in this mode than in any of the others; and that the corresponding variation of the frequency of the motion with the assumed frequency parameter was small.)

Results of the calculations of frequency and damping for the six modes of the wing are shown in Figs. 11 to 16. Results using aerodynamic coefficients for a constant frequency parameter of 0·26, obtained for direct comparison with results of the analogue computer investigation, are shown in Figs. 18 to 21.

7.4. *Calculation of the Effect of Changes in Humidity upon the Flutter Speed.*

It is pointed out in Section 3.2. that the foam plastic covering contributed substantially to the torsional stiffness of the wing, and to a smaller extent to the flexural stiffness, and that the stiffness of the plastic depended upon the absolute humidity of the surrounding air. Since the flutter speed of the wing varied rather more widely than would have been expected from a consideration of the possible experimental errors, an attempt was made to correlate the variation of the flutter speed and the absolute humidity. The prevailing humidity at the time of each flutter test was obtained from the records of the RAE weather station, and it was assumed that the humidity in the wind tunnel, which was vented to the atmosphere, was proportional to this. From a knowledge of the change in stiffness of the plastic with absolute humidity[6], and of the approximate contribution of the plastic to the torsional and flexural stiffness of the wing, estimates were made of the changes of the still-air frequencies of the wing over a range of variation of absolute humidity. These revised frequencies were then introduced into the flutter calculation and the corresponding critical speeds found. Fig. 17 shows the answers adjusted in mean level to pass through the experimental results. Taking account of the many uncertainties involved, there is fair agreement between the predicted and measured trends. Irrespective of the actual agreement obtained, however, the calculated results show how sensitive the flutter speed of this type of model can be to absolute humidity, and therefore how important it is to reduce as far as is practicable the contribution of the plastic to the total stiffness. Comments on the way this can be done are given in Section 9.

*Frequency parameter was defined as (angular frequency of oscillation) × (wing mean chord)/(wind speed).

8. *Comparisons of the Results of the Calculations and Measurements.*

8.1. *Wind-tunnel Measurements of Subcritical Response.*

Figs. 11 to 16 present the measured and calculated values of the model frequencies and fractions of critical damping plotted against windspeed.

For modes 2 and 3 the measured frequencies are in fairly good agreement with calculation over the full range of windspeed up to the critical condition. There is rather more experimental scatter in frequency for mode 1, but, again, the calculated values are broadly confirmed. In modes 4, 5 and 6 the limited number of frequency measurements taken substantiate the calculated results, which indicate that the frequencies of these modes remained practically unaltered throughout the speed range.

In many cases it proved difficult to obtain reliable estimates of damping from the measured vector-response curves at the higher windspeeds, and this is illustrated by the scatter and by the ranges of values given in Figs. 12, 13, 14 and 16. In mode 1, the measurements follow the trend of the calculated variation of damping with windspeed, although the mean of the experimental results is lower than the calculated results. In mode 2, the measured and calculated values are in very good agreement up to windspeeds of about 100 ft/sec; beyond this speed, in the region of peak damping, no satisfactory results were obtained owing to the high levels of tunnel turbulence, the unfavourable positions of the transducers and, possibly of the exciter, and the limited time available; over the range of speed in which the damping was falling rapidly, one measurement of good quality was taken, and this result in conjunction with the flutter point gives a trend of change of damping with windspeed that agrees well with calculation, although the critical speed could not, of course, be predicted from the subcritical response measurements made. In mode 3, problems of measurement were met similar to those encountered in mode 2, but a greater effort was made to position the acceleration transducer to give well-shaped response curves; the results obtained were not, however, by any means entirely satisfactory, but they do indicate a higher level for the peak damping than in the calculation, and that the peak occurred at a higher speed; there appear to be several possible reasons for this discrepancy, apart from experimental error, and these are discussed in Section 8.5. Fig. 16 shows that the dampings in modes 4, 5 and 6 increased slowly and steadily with windspeed, and that over the range in which measurements were taken the experimental and calculated results were in reasonable agreement.

8.2. *Prediction of the Flutter Condition from the Subcritical Response.*

It is of some interest to consider the prediction of the critical speed and frequency from the trend of variation of the subcritical response. It is clear modes 4, 5 and 6 play no significant part in the flutter motion. In mode 1 it did not prove possible to measure at all convincingly the marked increase in the rate of change of damping with windspeed above about 130 ft/sec that is apparent on the calculated curve, but if this curve had been followed then its behaviour should have been taken as an indication of the development of a significant amount of coupling between the original modes, and thus would have served as a warning of a potential instability. Mode 2 shows a calculated variation of damping with windspeed of the classical form for a mode leading to flutter; in this case also insufficient experimental results were obtained to define the curve; from an examination of the calculated result, however, it is apparent that with a certain amount of scatter in the values – and the greatest scatter would be expected at high damping – the reduction of damping with windspeed might not have been evident until the damping was low; this emphasises the importance of making measurements at small increments in speed. Fig. 14 shows the variation of damping with windspeed in mode 3; the experimental results give a clear indication of an approach to flutter, but this prediction is misleading; as it happened, the measured damping trend from mode 3 would have given a reliable estimate of the actual flutter speed, but ciné records of the model motion up to and at flutter, and the frequencies, leave little room for doubt that the flutter occurred in mode 2.

The variations with windspeed of the frequencies in modes 1, 2 and 3 are given in Fig. 11; for this wing, the frequency curves appear to be of no help in predicting the flutter, and, indeed, if the results for modes 2 and 3 were extrapolated on the assumption that the critical condition occurred at the point where the curves intersected and the frequencies coincided, then the flutter speed would have been overestimated.

8.3. *Analogue Measurements of Subcritical Response.*

The results of analyses of the vector-response measurements taken on the flutter simulator are shown in Figs. 18 to 21 together with the exact calculated solutions of the equations of free motion. Although there is inevitably some scatter in the values obtained using the analogue approach, generally the two sets of results are in good agreement; the biggest discrepancies occur at the highest levels of the damping, and in mode 3 the analogue answers in the region of peak damping are about 15 per cent higher than the exact solutions.

In Ref. 3 Broadbent and Hartley describe a theoretical investigation in which the damping rates for a binary system were deduced from the calculated shapes of the vector response curves; comparison with the exact solution showed scatter of about ± 20 per cent in the neighbourhood of the peak damping. Since this investigation was not subject to the errors that can arise in using an analogue computer, the discrepancies of about 15 per cent in the present series of calculations are evidently not unduly high, and probably merely indicate the difficulties of obtaining accurate values for damping from vector response curves.

8.4. *The Critical Flutter Condition.*

The mean of the measured flutter speeds was 168 ft/sec and the frequency was 6·6 c/sec. The calculations were made using mode frequencies appropriate to the condition in which a speed was measured equal to the mean speed; the resultant calculated flutter speed was 165 ft/sec and the frequency was 6·4 c/sec. The agreement is considered good.

8.5. *Discussion of Possible Reasons for the Discrepancies between the Observed and Calculated Subcritical Response.*

The main evidence of a discrepancy between the observed and calculated behaviour of the model is the difference between the damping curves for mode 3, shown in Fig. 14. There are two main sources for error on the theoretical side. One of these is that the theoretical model of the structure was inaccurate, and the other is that the representation of the aerodynamic forces was inaccurate.

Dealing with the structural representation, the model was treated as a system with six degrees of freedom, each degree of freedom being a mode deduced from the still-air response measurements. Although this point was not pursued, comparisons indicated that there were some differences between the vector response of the theoretical system under simulated excitation and the measured response of the actual model in still air. An attempt to resolve this matter would involve the whole question of the interpretation of vector response curves, and this is beyond the scope of the present Report.

The theoretical aerodynamic forces could be in error for a variety of reasons. Wind-tunnel interference may have been significant, for example, particularly since it is not an ideal arrangement to mount a half model on a reflector plate at the boundary of a circular-section, open-jet wind tunnel; it would be possible, in principle, to check on the interference effect by repeating the tests with the model mounted from one wall of a closed-section rectangular tunnel; such a tunnel might have the additional merit of providing a windstream with lower turbulence.

9. *Ways of Reducing the Contribution of the Plastic Foam to the Structural Stiffness of the Model.*

The contribution of the plastic foam to the torsional stiffness of the wing arose principally from the severe local deformation of the plastic that occurred between the segments in the region of the trailing edge when the wing was twisted. The deformation in these areas could have been reduced by increasing the width of the gap between segments but this would have increased the deflection of the plastic between the supporting metal segments under the aerodynamic loading. The width of the gap chosen was therefore a compromise based on the anticipated aerodynamic loading, the stiffness of the plastic and some arbitrary permissible deflection. It later became clear that on this model a much wider gap could have been allowed, since the aerodynamic loading had been overestimated and the stiffness of the foam underestimated.

The contribution of the foam to the overall stiffness could also have been reduced by taking a lower thickness to chord ratio for the wing section. Since the model was tested at nominally zero incidence this would probably not have altered the oscillatory aerodynamic forces significantly.

10. *Conclusions.*

A series of measurements has been made of the displacement-vector response of an aeroelastic swept-wing model under sustained sinusoidal excitation at windspeeds below the critical flutter speed. From the curves showing the variation with frequency of the amplitude and phase of the motion relative to the exciting force, values have been determined for the damping and frequency of the natural modes of oscillation, based on the assumption that the response takes the same general form as the response of a system with a single degree of freedom.

The measured reponse of the model at subcritical speeds and its flutter characteristics were compared with calculated results. Good agreement was obtained on the flutter speed and frequency; the frequencies of the natural modes at subcritical speeds were also generally in good agreement, but there were discrepancies between the associated dampings in the modes. The differences may have been due to difficulties in measuring the response in the presence of high turbulence in the wind tunnel; wind-tunnel interference may also have been a contributory factor.

Experience gained in the tests emphasises the importance of the following factors in measurements of subcritical response:

(i) Turbulence in the windstream can lead to difficulties in obtaining response curves that are accurate enough to yield reliable values of the damping and frequency of the natural modes: it is therefore very desirable that the means of excitation should be powerful enough to give a level of forced response that is high in relation to the response to turbulence; the power required in any particular case is dependent upon the characteristics of the equipment used to measure the amplitude and phase of the displacement response.

(ii) A system of excitation that gives an adequate forced response in the modes of oscillation in still air may not be satisfactory with the wind on, due to the changes in mode shapes.

(iii) The quality of the response curves depends upon the position on the model at which measurements are taken, and consequently it is an advantage to be able to examine the response at many positions.

(iv) Equipment to measure model displacement and present the results plotted in the form of vector response curves is of great value (such equipment – not the first of its kind in the U.K.[1,11] – is now in use at RAE).

A new method was used in the construction of the model. A structure comprising a metal spar with rib members attached to it was covered with soft plastic, foamed in position; this technique appears to offer certain advantages in building aeroelastic models for test at low subsonic speeds, but it is important to arrange for the contribution of the plastic to the structural stiffness of the model to be kept to a minimum.

LIST OF REFERENCES

No.	*Author(s)*	*Title, etc.*
1	C. Scruton and E. P. L. Windsor	Flutter investigations in high speed wind tunnels. Rep. NPL/Aero/360. 1958.
2	C. C. Kennedy and C. D. P. Pancu	Use of vectors in vibration measurement and analysis. *J. Aero. Sci. 14*, No. 11, 603–625. 1947.
3	E. G. Broadbent and E. V. Hartley	Vectorial analysis of flight flutter test results. A.R.C. R. & M. 3125. February 1958.
4	G. M. L. Gladwell and R. E. D. Bishop ..	An investigation into the theory of resonance testing. A.R.C. 22,381. September 1960.
5	D. L. Woodcock	On the interpretation of the vector plots of forced vibrations of a linear system with viscous damping. *Aeronaut. Q. 14*, 45–62. 1963.
6	D. B. Payen	Stiffness, damping and creep properties of a polyurethane foam including the effects of temperature and humidity. A.R.C. C.P. 905.
7	S. C. Redshaw and P. J. Palmer	The construction and testing of a Xylonite model of a delta aircraft. *Aeronaut. Q. 3*, 83–127. 1951.
8	P. R. Guyett and C. A. K. Irwin	Measurements of the vector response of a swept wing model in still air. A.R.C. 24,215. November 1962.
9	H. Templeton	The technique of flutter calculations. A.R.C. C.P. 172. April 1953.
10	W. D. T. Hicks	An electric analogue computer representing twelve coupled linear differential equations. A.R.C. R. & M. 3495.
11	W. R. Wignall	Automatic low frequency response editing device (ALFRED). A.R.A. Instrumentation Laboratory Memo No. 4. 1960.

TABLE 1

Dimensions of Spar and Segments (see Fig. 2).

Perpendicular distance of station from root, inches	A Width of each spar member, inches	B Overall width of spar, inches	C Width of chamfer at trailing edge of segment, inches
0	—	3·00	1·84
2	—	2·87	1·84
4	1·26	2·74	1·84
6	1·15	2·61	1·84
8	1·04	2·49	1·84
10	0·93	2·36	1·84
12	0·84	2·23	1·84
14	0·75	2·10	1·84
16	0·68	1·98	1·84
18	0·60	1·85	1·84
20	0·53	1·72	1·84
22	0·45	1·59	1·90
24	0·38	1·46	1·955
26	0·34	1·34	2·015
28	0·28	1·21	2·07
30	0·20	1·08	2·130
32	0·16	0·95	2·185
34	0·13	0·82	2·245
36	—	0·70	2·30

TABLE 2

Mass Distribution in Model.

Section	Distance of C/L of section from root, inches	Mass, slugs	Distance of centroid of section from leading edge, inches	Radius of gyration in pitch about the centroid, inches
1	1	0·0252	9·19	5·04
2	3	0·0238	8·85	4·85
3	5	0·0222	8·49	4·65
4*	7	0·0224	8·85	4·72
5	9	0·0192	7·73	4·23
6	11	0·0178	7·36	4·01
7	13	0·0162	6·99	3·81
8	15	0·0148	6·62	3·60
9	17	0·0138	6·24	3·40
10	19	0·0124	5·88	3·19
11	21	0·0110	5·49	2·97
12	23	0·0096	5·13	2·78
13	25	0·0086	4·74	2·55
14	27	0·0072	4·36	2·34
15	29	0·0064	3·96	2·11
16	31	0·0054	3·54	1·92
17	33	0·0044	3·16	1·71
18	35	0·0032	2·81	1·51

*Includes attached exciter parts

TABLE 3

Inertia Matrix for Modes Based on Circle Diameters: Values Given in Slugs for Unit Displacement in Modes at Wing Leading Edge 35 inches from the Root.

0·026217	−0·000665	−0·000142	−0·000323	−0·000958	0·001353
−0·000665	0·025269	0·000627	−0·002866	0·000997	0·000139
−0·000142	0·000627	0·030055	−0·000014	0·001473	0·001807
−0·000323	−0·002866	−0·000014	0·091499	−0·002445	0·002761
−0·000958	0·000997	−0·001473	−0·002445	0·026231	−0·004457
0·001353	0·000139	0·001807	0·002761	−0·004457	0·019146

TABLE 4

Orthogonality Check on Inertia Matrix.

1·000	−0·026	−0·005	−0·007	−0·037	0·060
−0·026	1·000	0·023	−0·060	0·039	0·006
−0·005	0·023	1·000	−0·000	−0·052	0·075
−0·007	−0·060	−0·000	1·000	−0·050	0·066
−0·037	0·039	−0·052	−0·050	1·000	−0·199
0·060	0·006	0·075	0·066	−0·199	1·000

TABLE 5

Modal Frequencies and Fractions of Critical Damping in Still-air.

No.	Mode	Frequency c/s	Fractions of critical damping C/C_c
1	Fundamental bending	1·735	0·017
2	1st overtone bending	7·23	0·017
3	Fundamental torsion	14·75	0·028
4	2nd overtone bending	17·50	0·018
5	3rd overtone bending	31·1	0·022
6	1st overtone torsion	32·9	0·053
7	4th overtone bending	47·5	—

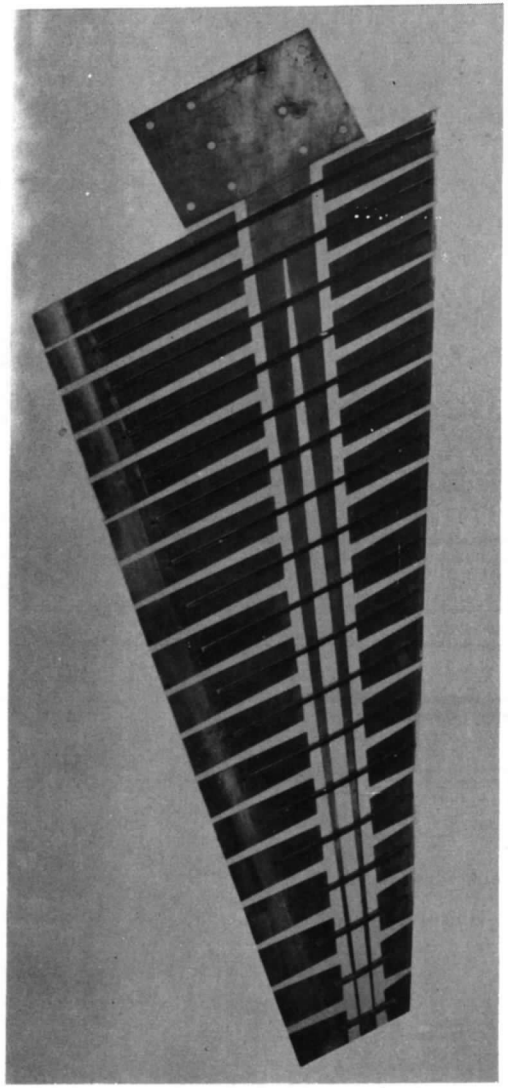

FIG. 1a. Swept-wing; spar and segments.

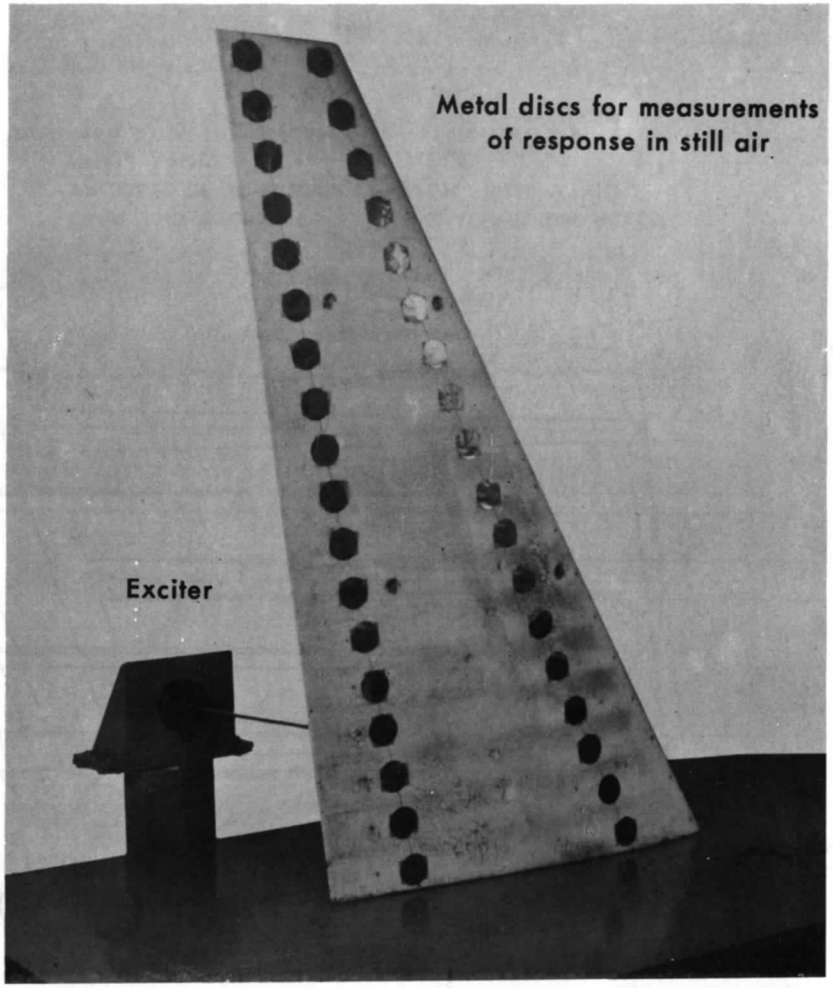

FIG. 1b. Swept-wing model on wind-tunnel mounting.

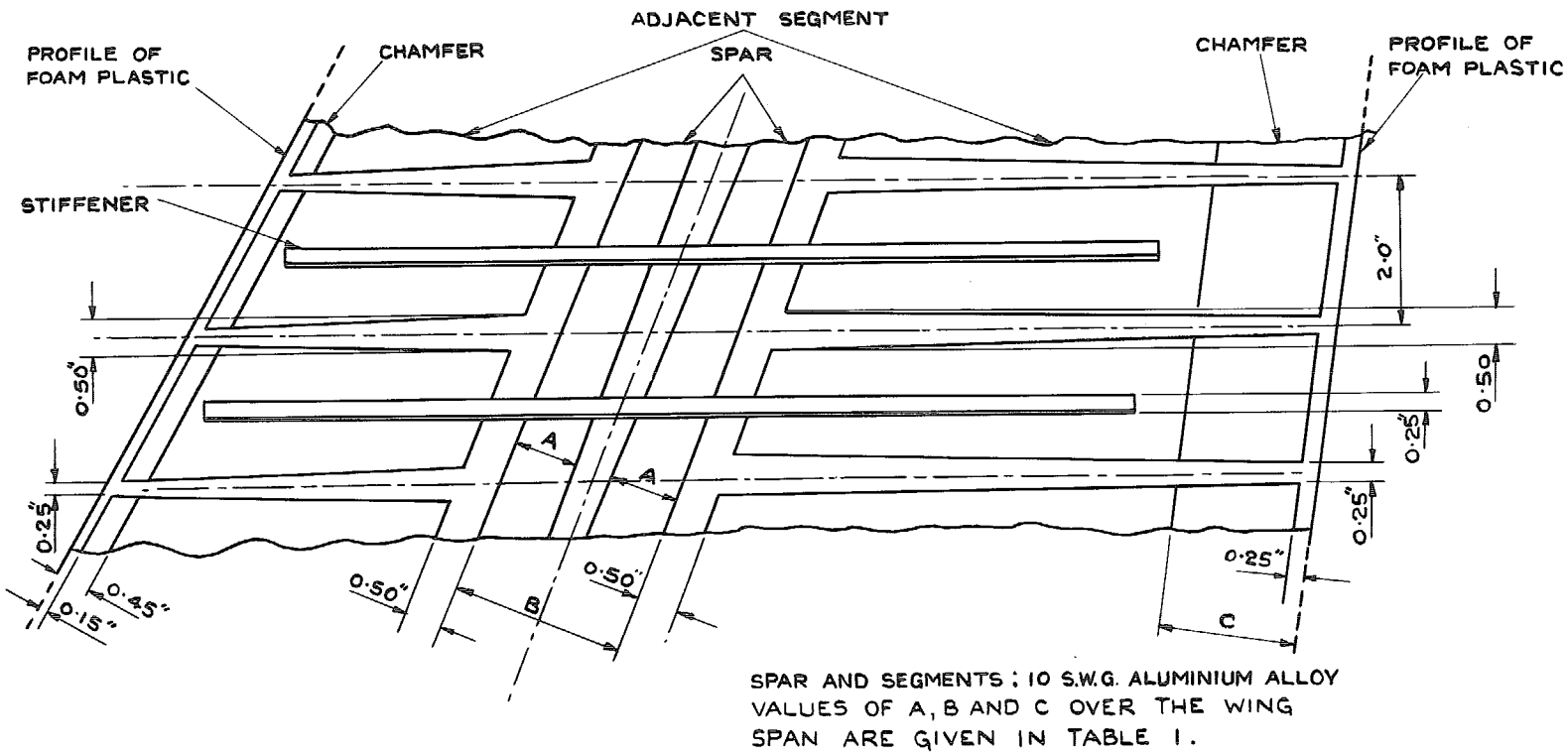

FIG. 2. Typical part of model structure.

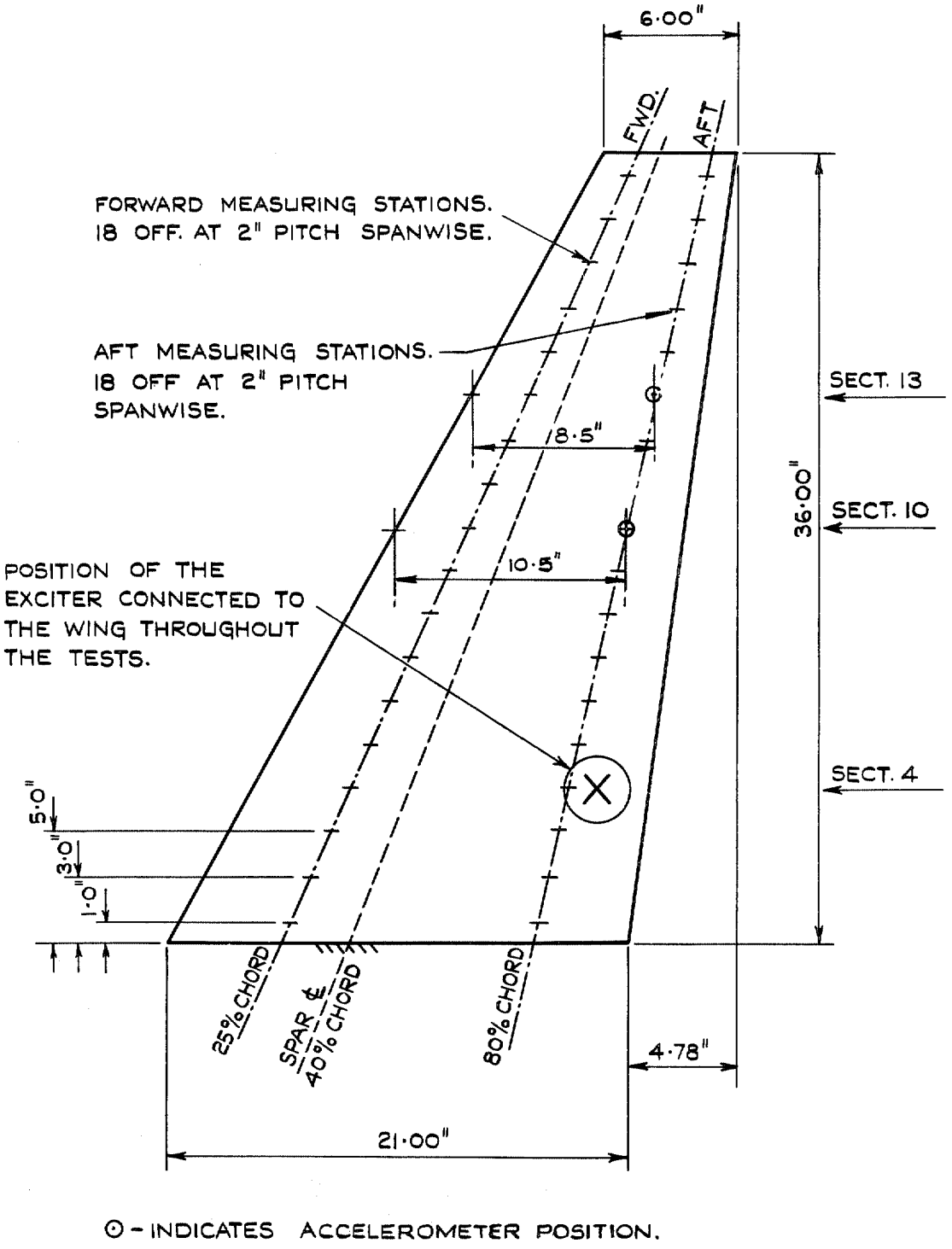

FIG. 3. Arrangement of excitation and amplitude measurement stations.

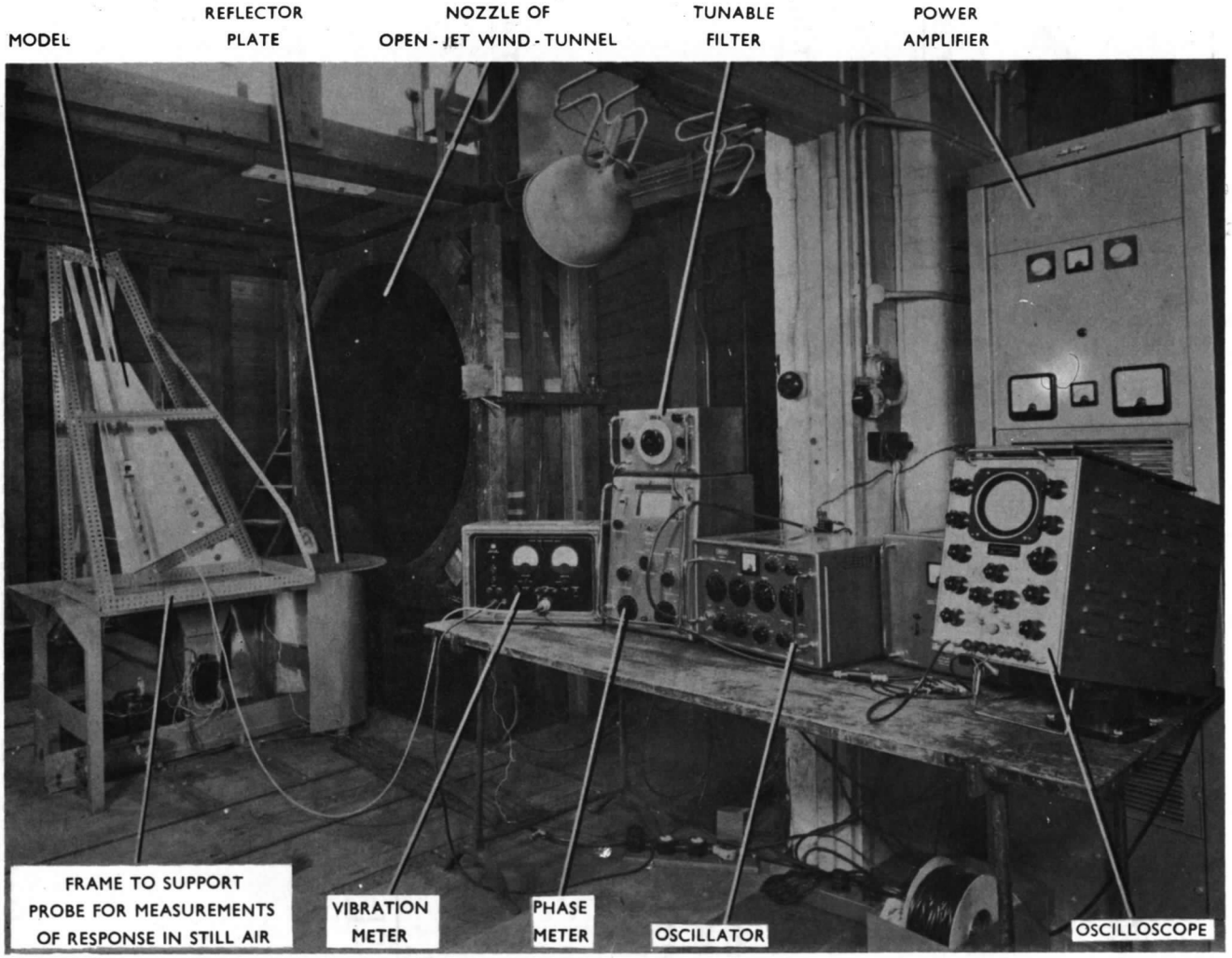

FIG. 4. Arrangement of apparatus in wind tunnel.

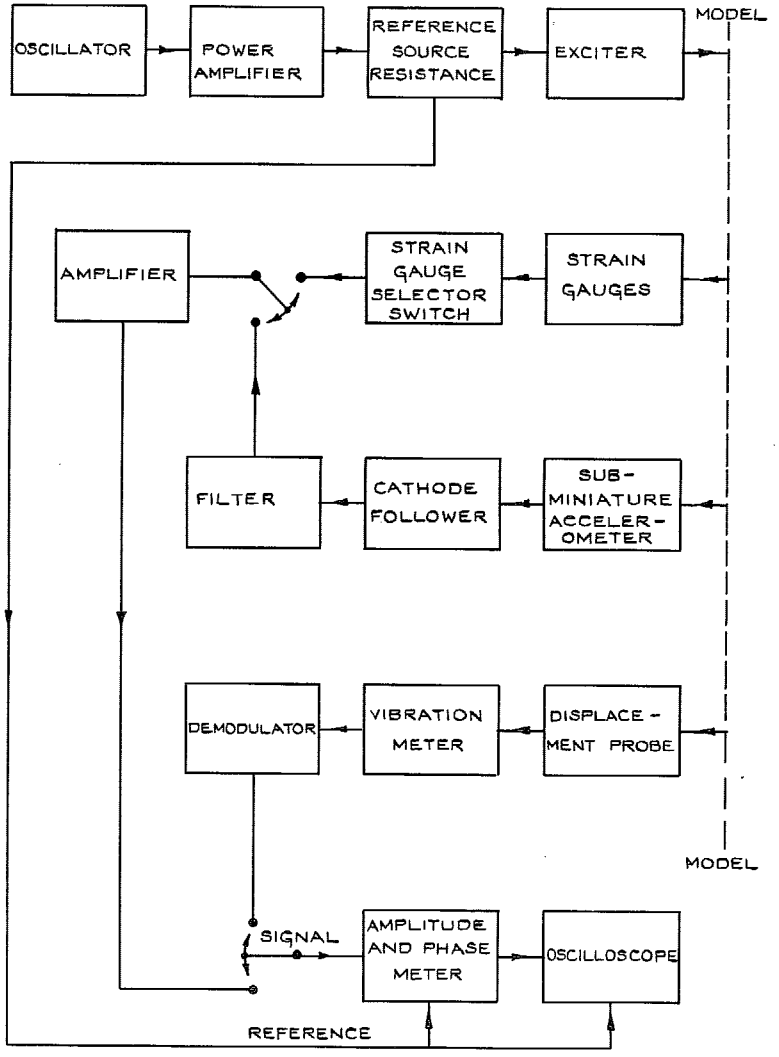

FIG. 5. Apparatus for excitation and measurement of response of swept-wing model.

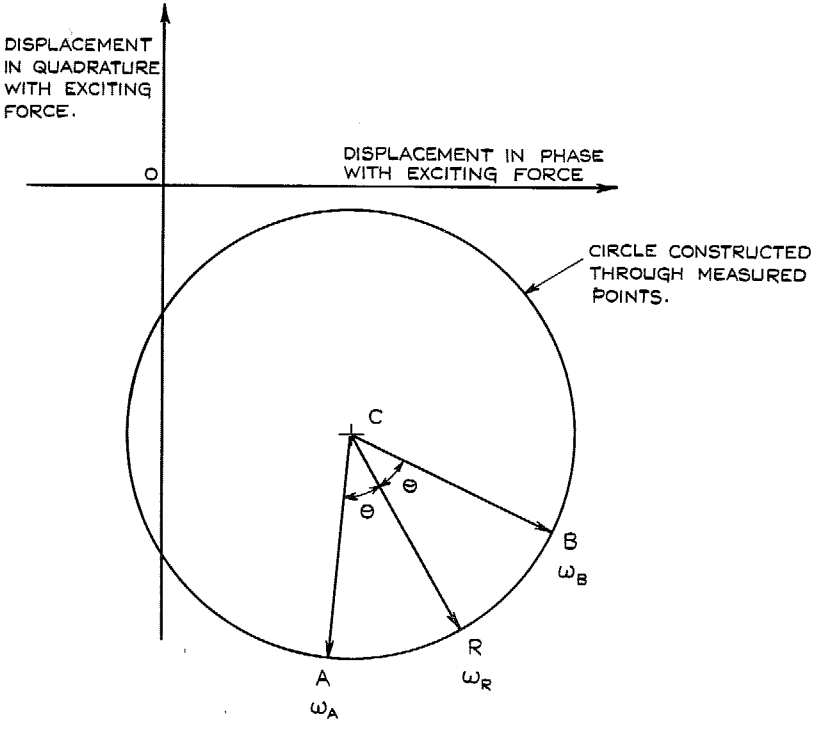

FIG. 6. Method of analysis of a vector-response plot.

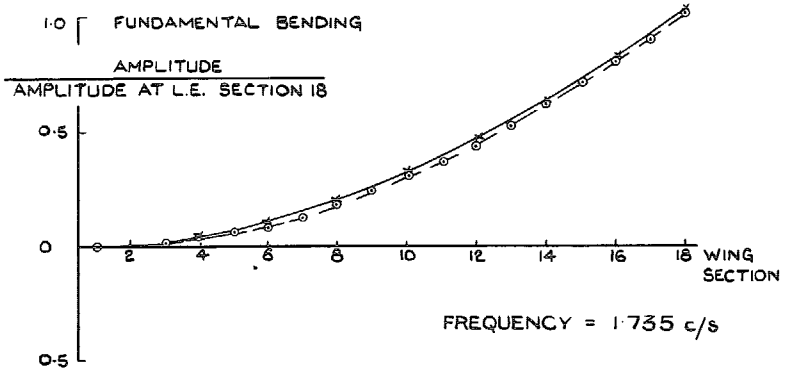

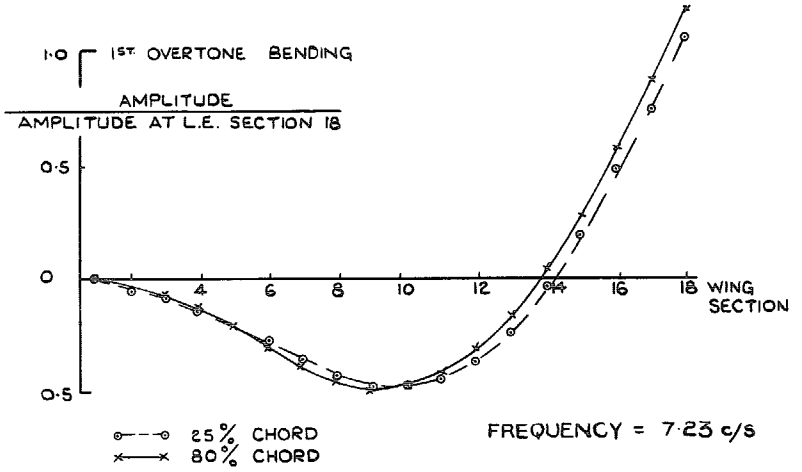

Results based on vector-response plot circle diameters.

FIG. 7. Fundamental bending and 1st overtone bending modes.

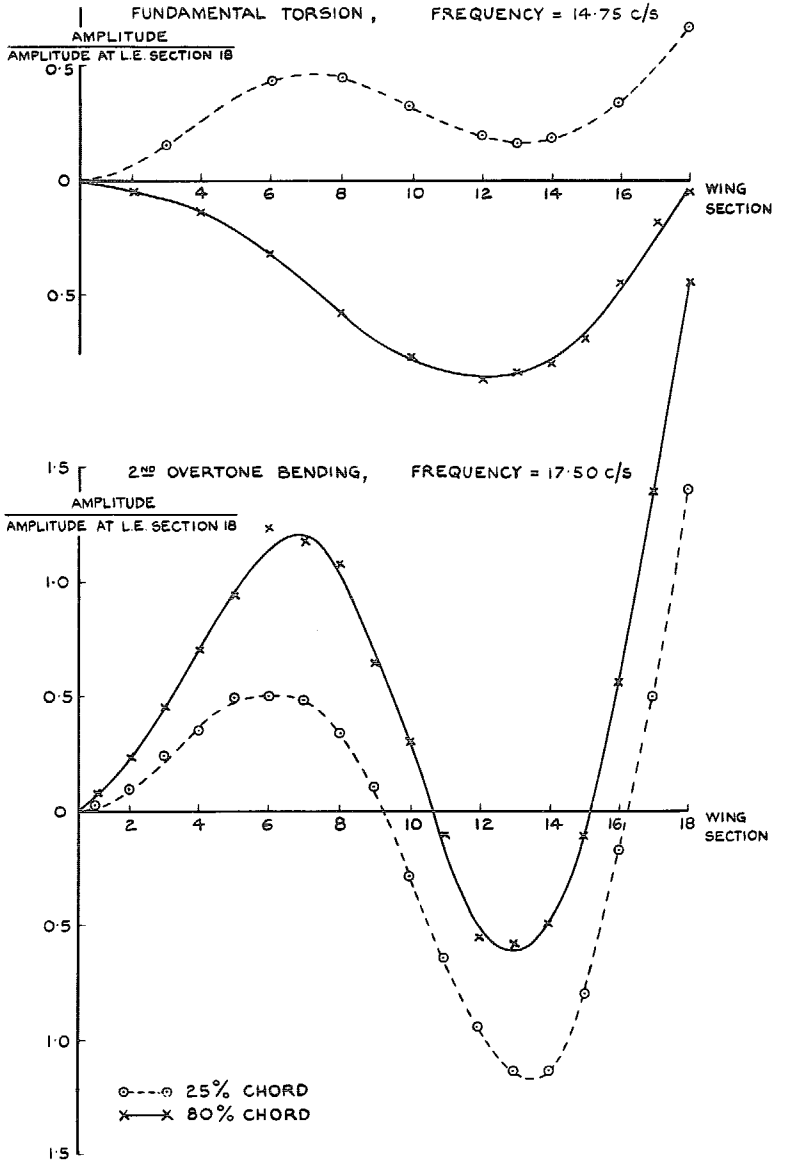

Results based on vector response-plot circle diameters.

FIG. 8. Fundamental torsion and 2nd overtone bending modes.

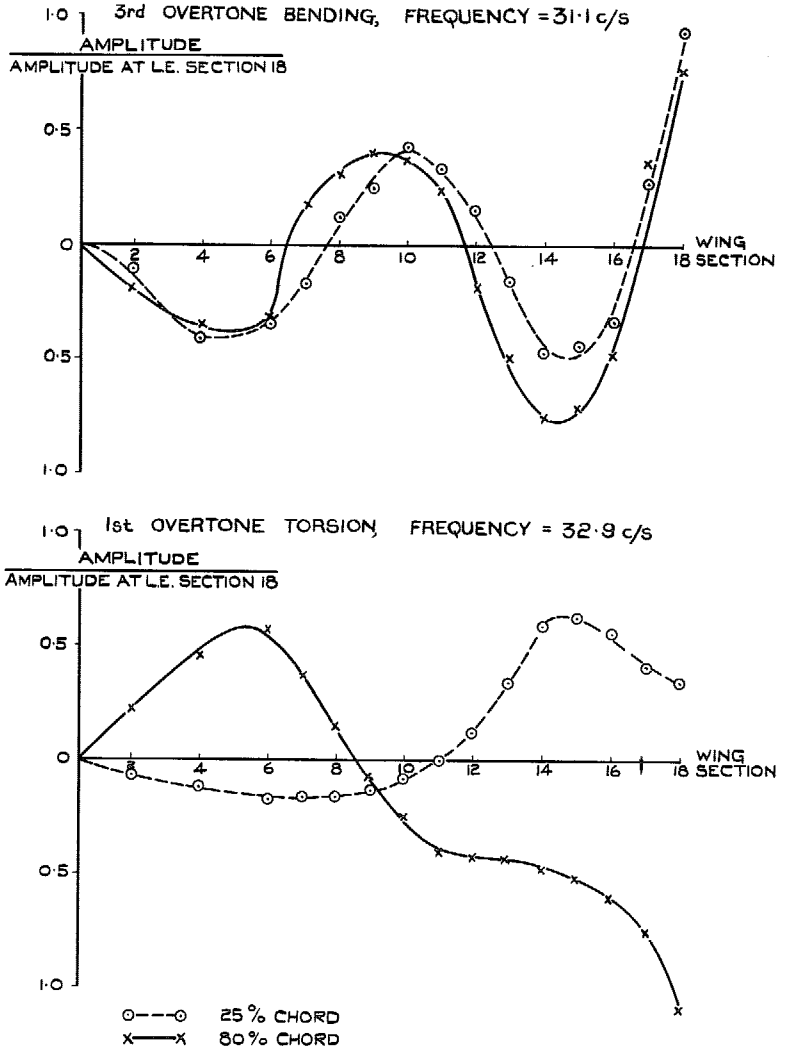

FIG. 9. 3rd overtone bending and 1st overtone torsion modes.

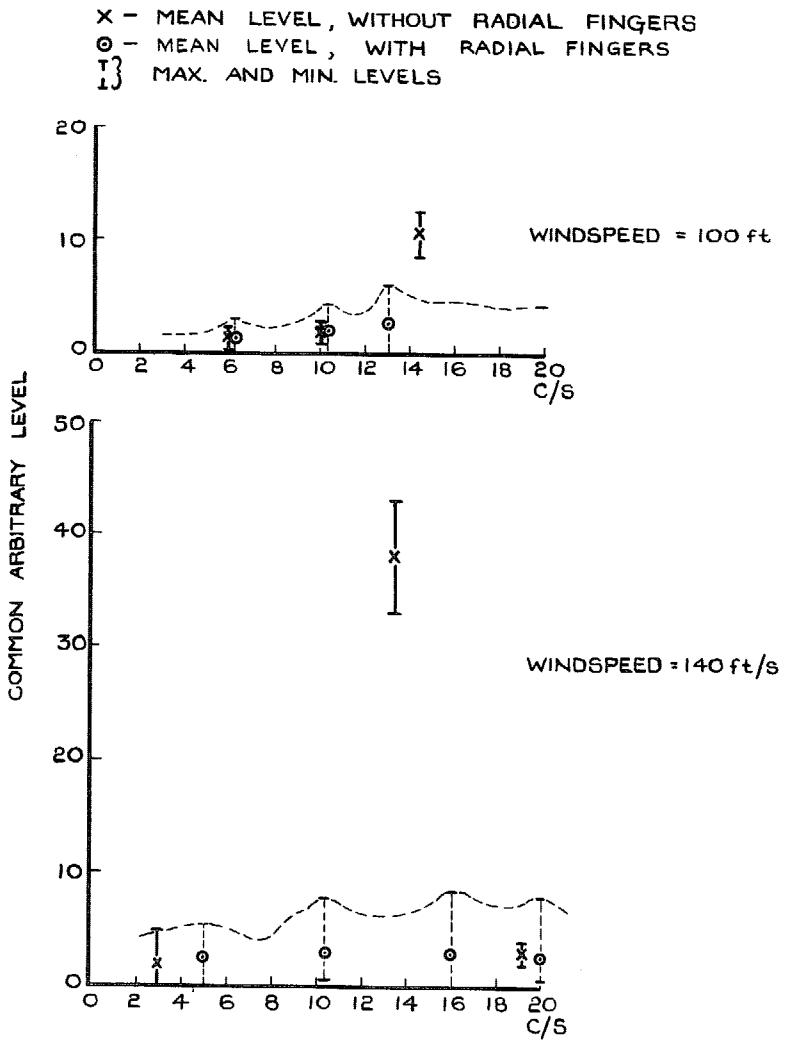

FIG. 10. Peak levels of wind-tunnel turbulence at 100 ft/sec and 140 ft/sec.

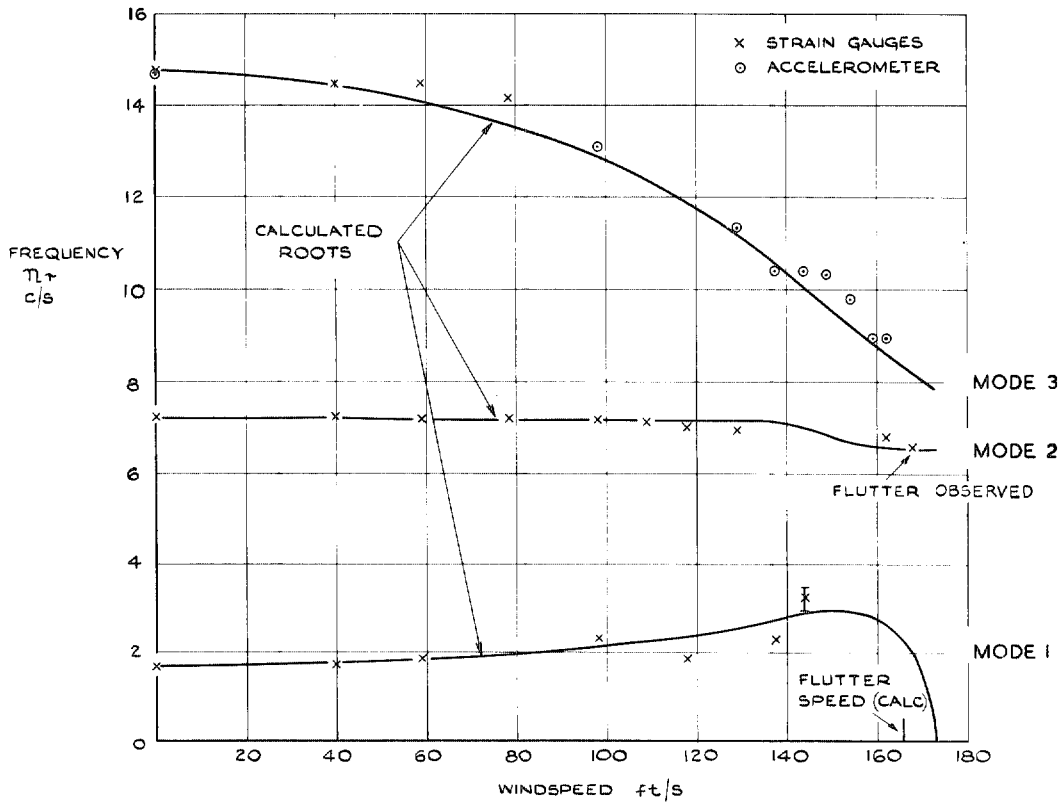

FIG. 11. Variation of modal frequencies with windspeed for modes 1 to 3.

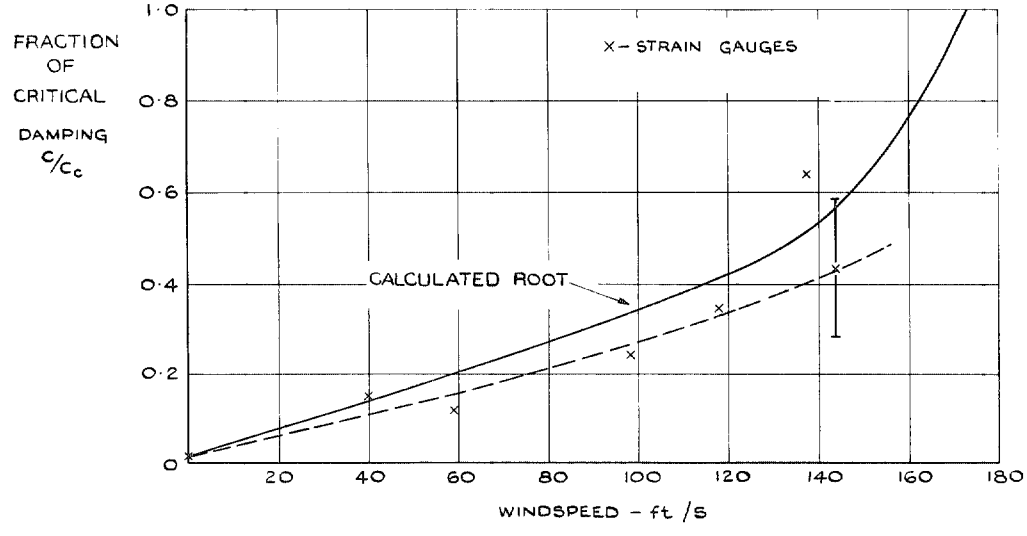

FIG. 12. Variation of modal damping with windspeed for mode 1.

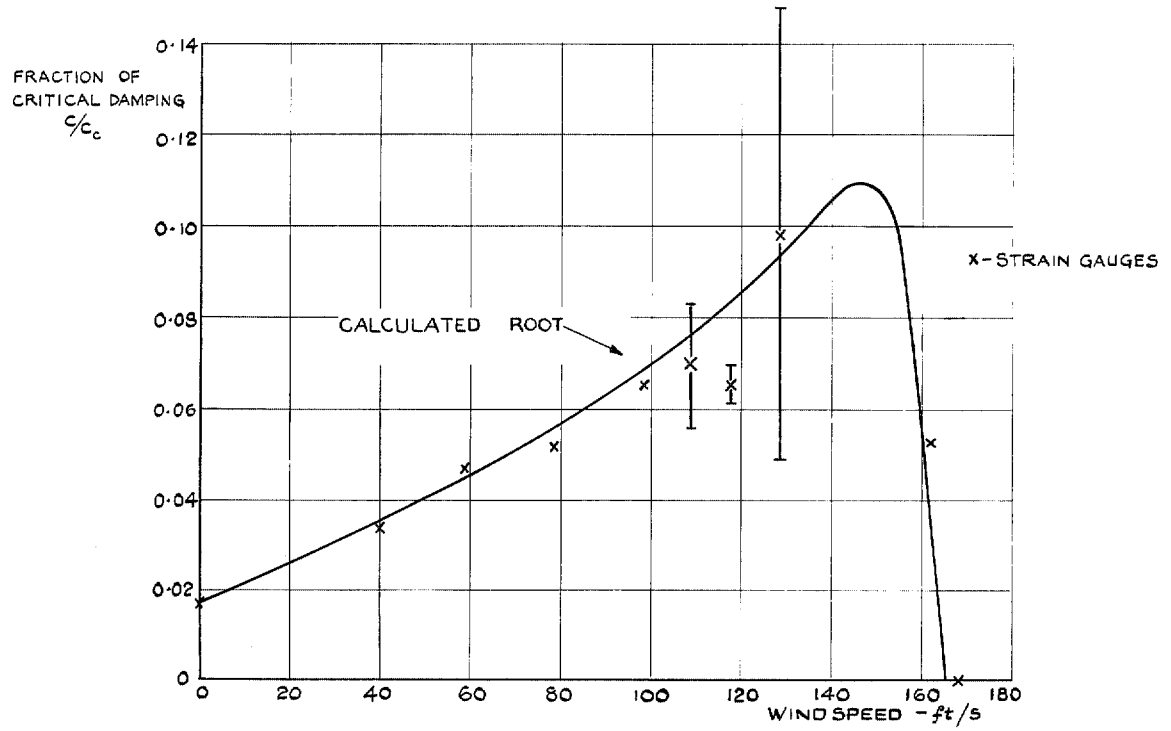

FIG. 13. Variation of modal damping with windspeed for mode 2.

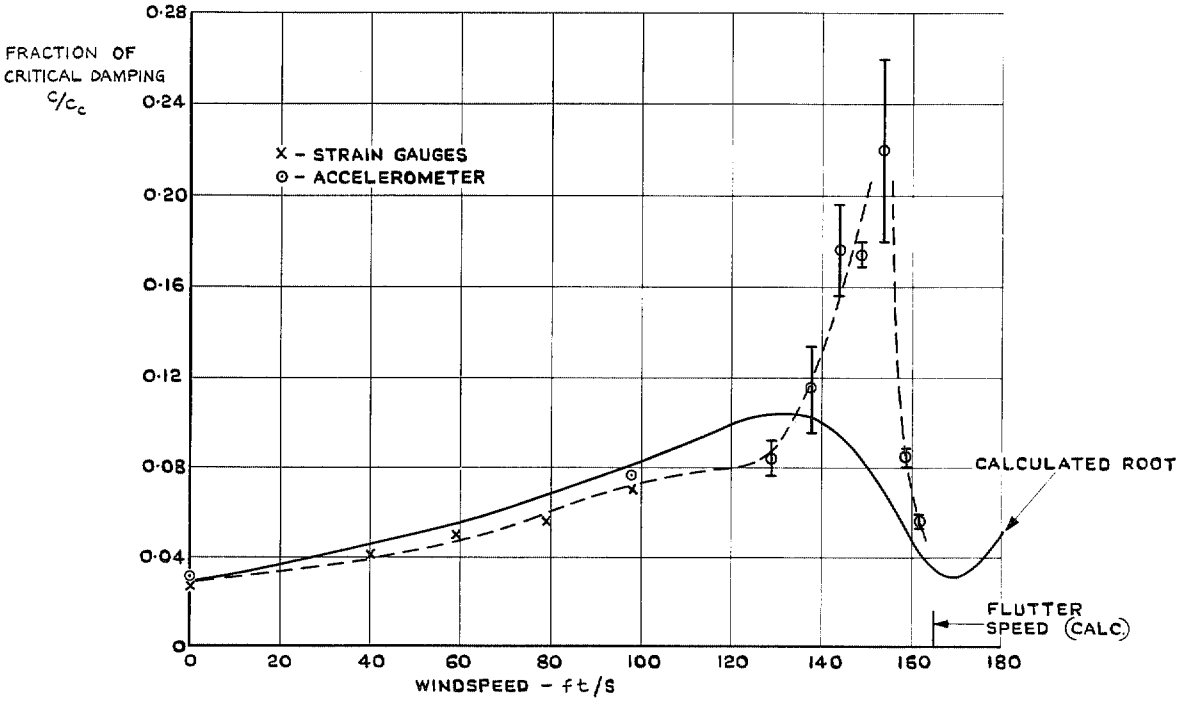

FIG. 14. Variation of modal damping with windspeed for mode 3.

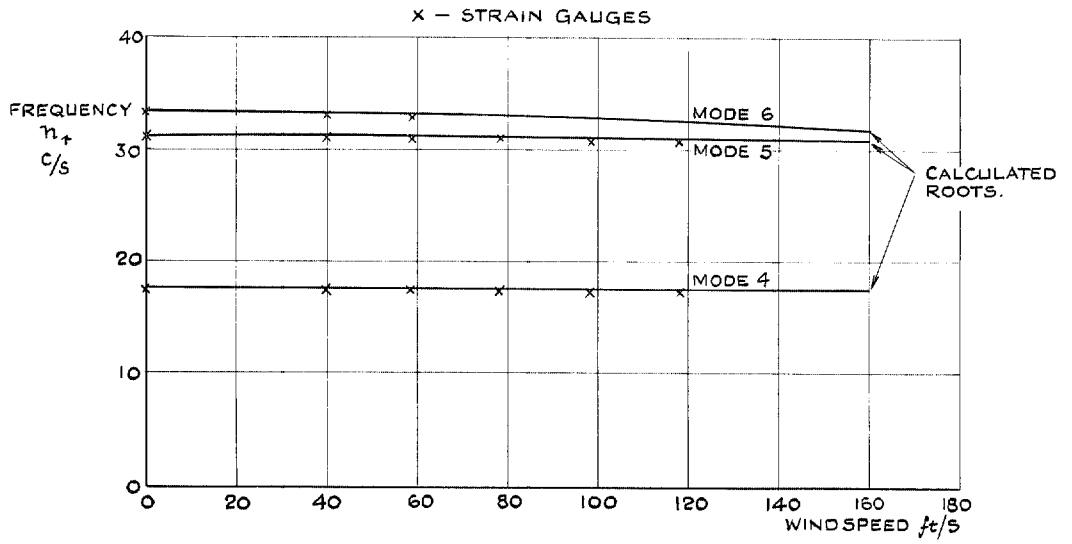

FIG. 15. Variation of modal frequencies with windspeed for modes 4 to 6.

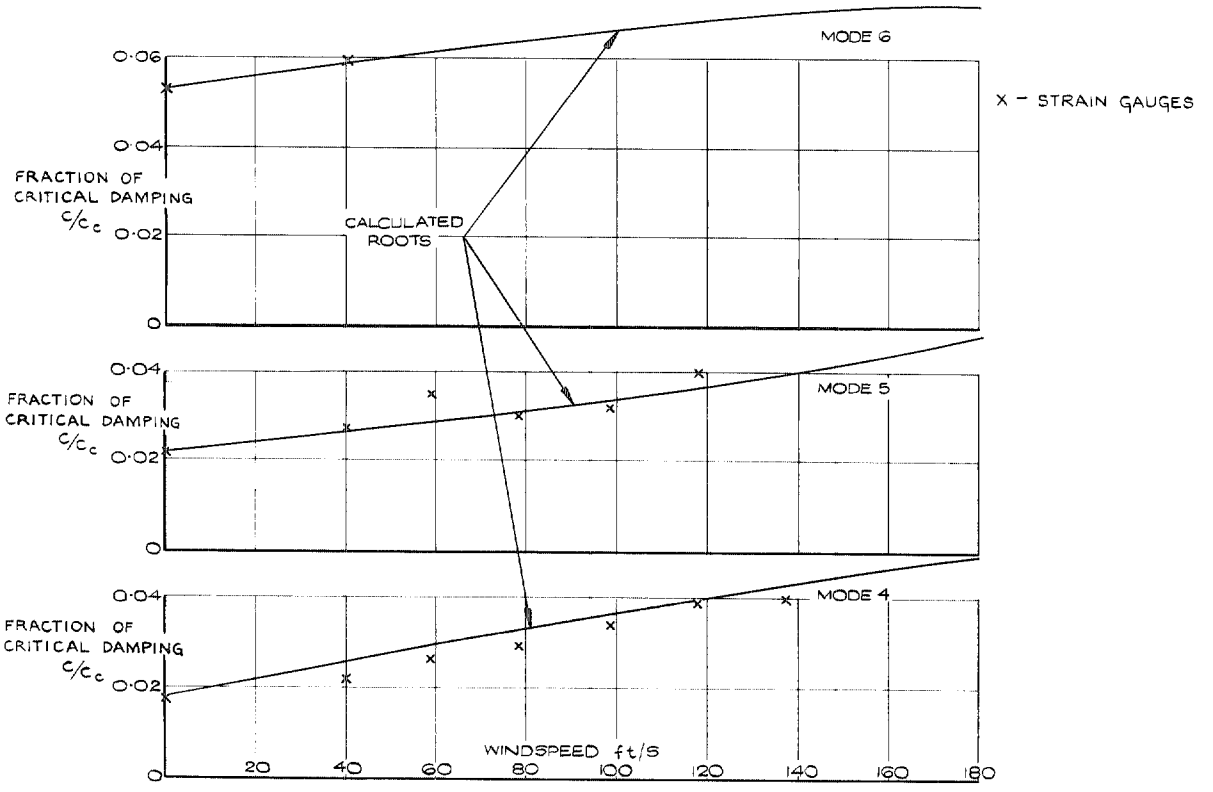

FIG. 16. Variation of modal damping with windspeed for modes 4 to 6.

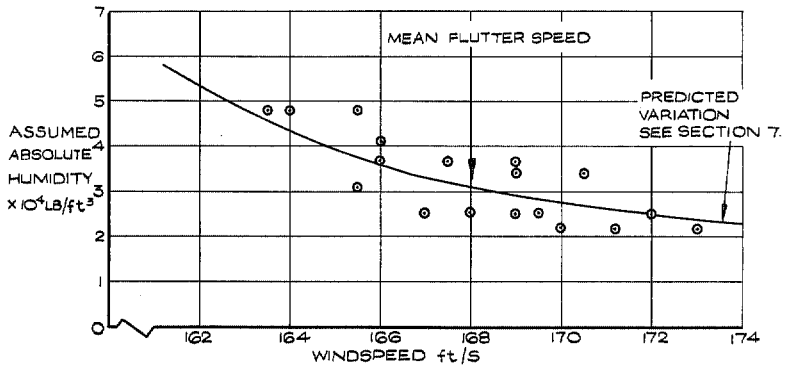

FIG. 17. Effect of absolute humidity on flutter speed.

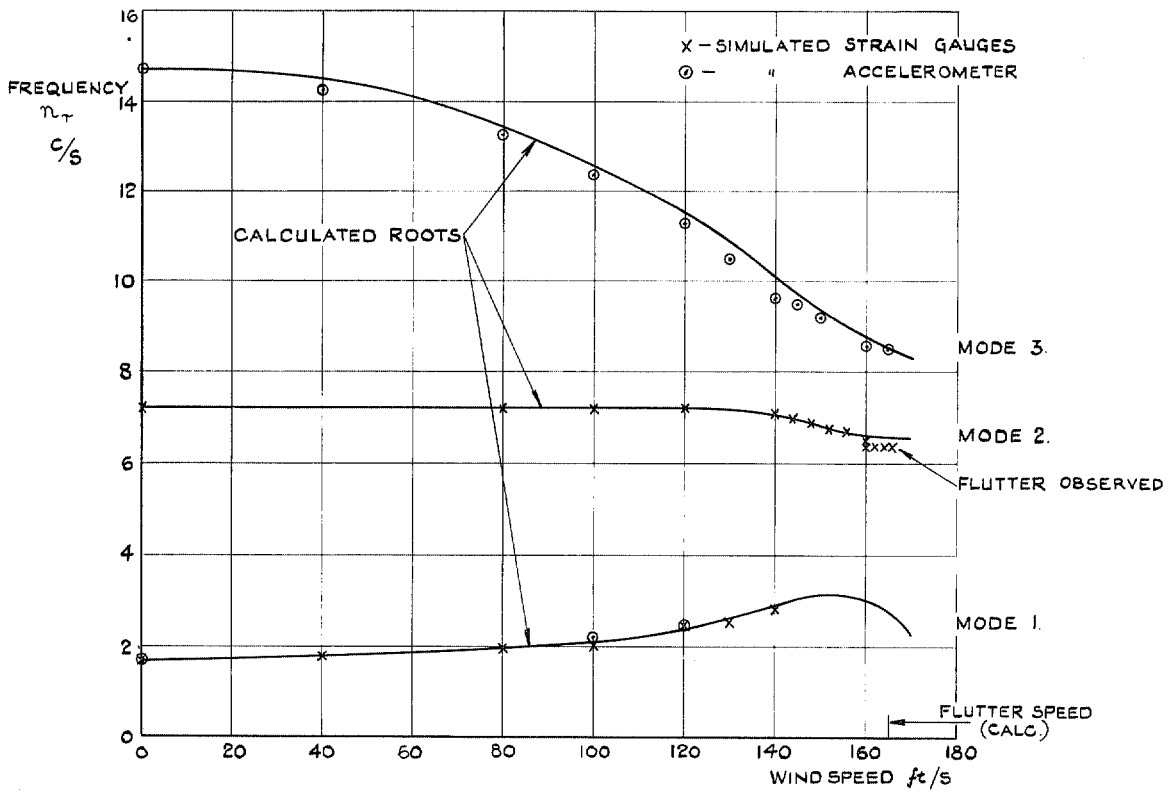

FIG. 18. Variation with windspeed of modal frequencies obtained from analogue computer (with constant frequency parameter).

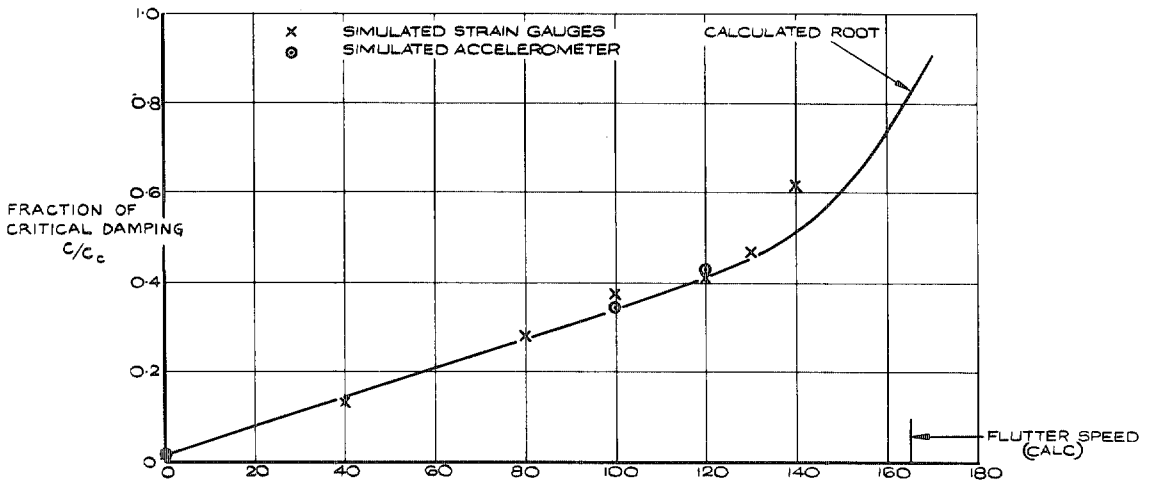

FIG. 19. Variation with windspeed of modal damping obtained from analogue computer for mode 1. (With constant frequency parameter).

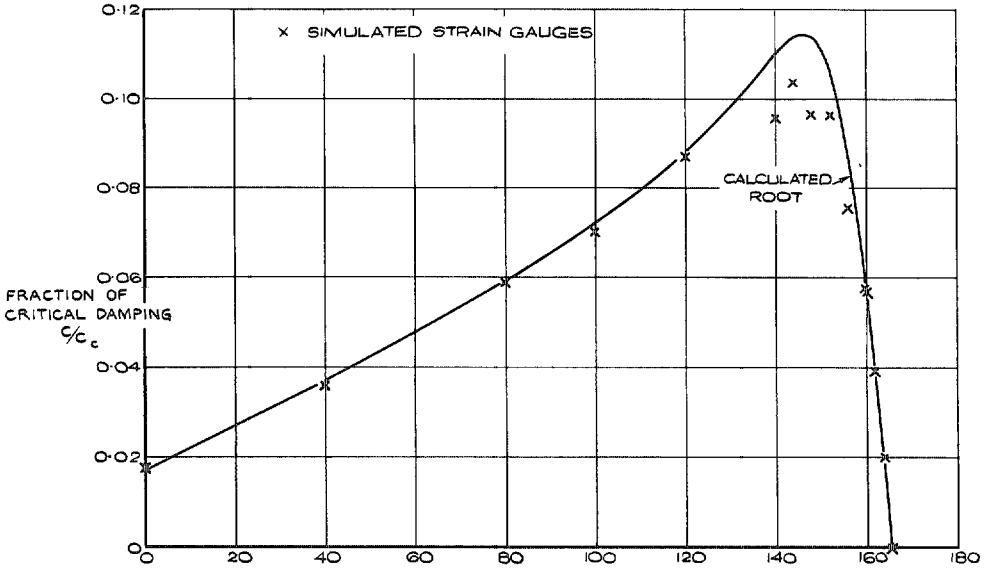

FIG. 20. Variation with windspeed of modal damping obtained from analogue computer for mode 2. (With constant frequency parameter).

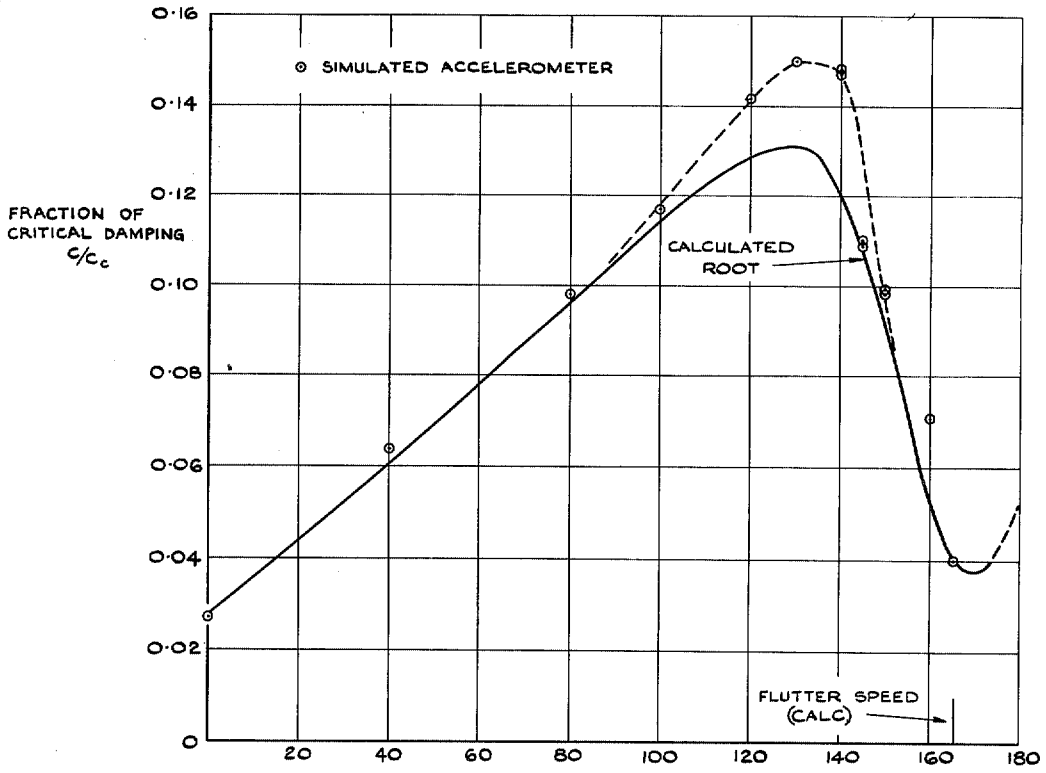

FIG. 21. Variation with windspeed of modal damping obtained from analogue computer for mode 3. (With constant frequency parameter).

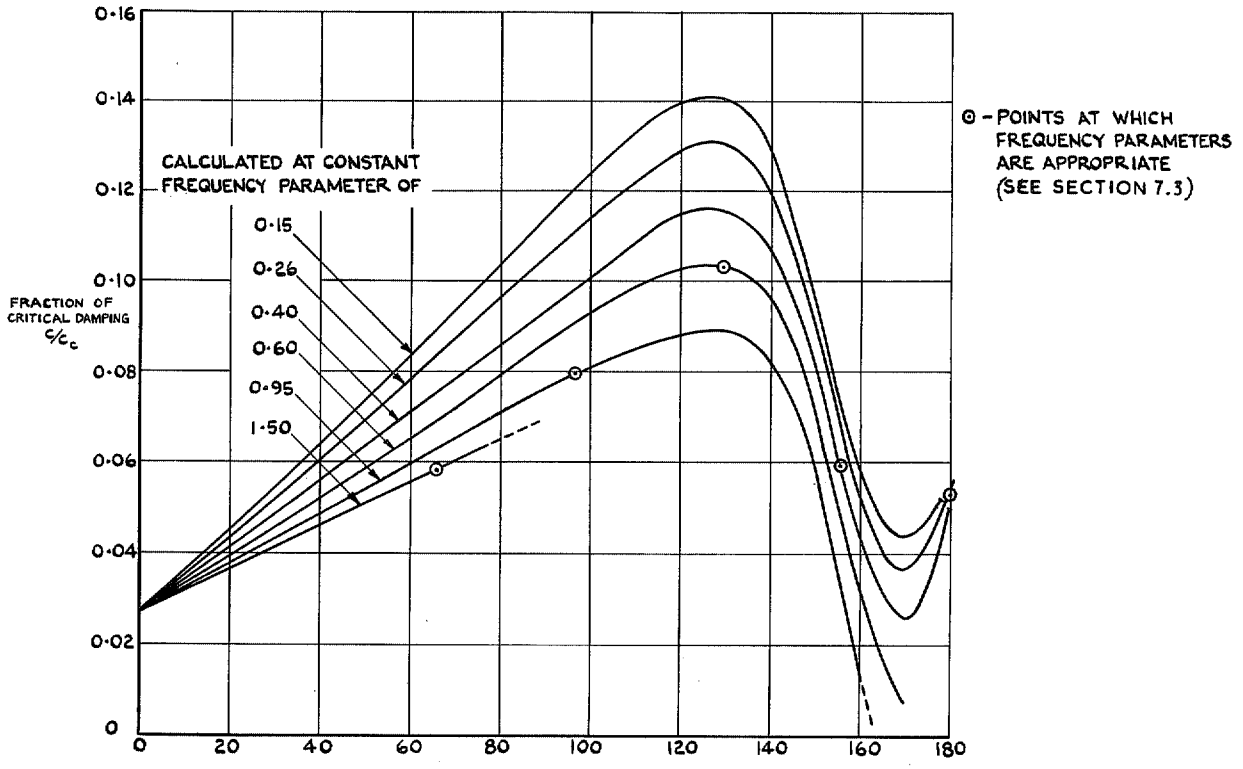

FIG. 22. Effect of frequency parameter on calculated modal damping for mode 3.

Printed in Wales for Her Majesty's Stationery Office by Allens Printers (Wales) Limited.

Published by
HER MAJESTY'S STATIONERY OFFICE

To be purchased from
49 High Holborn, London W.C.1
423 Oxford Street, London W.1
13A Castle Street, Edinburgh 2
109 St. Mary Street, Cardiff, CF1 1JW
Brazennose Street, Manchester 2
50 Fairfax Street, Bristol 1
258–259 Broad Street, Birmingham 1
7–11 Linenhall Street, Belfast, BT2 8AY
or through any bookseller

R. & M. No. 3497

S.O. Code No. 23-3497